Acta metall. Vol. 31, No. 11, pp. 1781–1793, 1983
Printed in Great Britain.

0001-6160/83/ $3.00 + 0.00

OVERVIEW NO. 30

GASEOUS HYDROGEN EMBRITTLEMENT IN FeSi- AND Ni-SINGLE CRYSTALS

H. VEHOFF and W. ROTHE
Max-Planck-Institut für Eisenforschung, Düsseldorf, FRG

(*Received* 21 *April* 1983)

Abstract—Hydrogen embrittlement in FeSi- and Ni-single crystals was examined at low hydrogen pressures (10 mPa $\leqslant p\mathrm{H}_2 \leqslant$ 100 kPa). A special technique was used to measure the crack tip opening angle α of a stable growing crack as a function of temperature, hydrogen pressure and rate. The relationship between α and the crack tip opening rate depends on temperature. Three temperature regions can be distinguished, at low temperatures (below 293 K) transport processes control embrittlement, at intermediate temperatures (293 K $\leqslant T \leqslant$ 390 K) hydrogen embrittlement is controlled by the equilibrium concentration of hydrogen in the fracture process zone and at even higher temperatures brittle crack nucleation becomes difficult. The detailed microscopic processes which occur during hydrogen embrittlement are examined using *in situ* SEM crack propagation studies and SEM fractography. These results as well as examinations of the influence of oxygen–hydrogen mixtures on the fracture process show that the fracture process occurs at a distance of less than 100 nm from the crack tip. Models of hydrogen embrittlement which relate embrittlement either to the decrease of the surface energy or to the increase of hydrogen concentration in the fracture process zone or to the hydrogen coverage at the crack tip are discussed and compared with the experimental results. To explain the results it is assumed that hydrogen embrittlement can be related to the fractional coverage of a special site at the tip of a stressed crack. With this assumption the measurements of the $p\mathrm{H}_2$ and T dependence of α yield that this site can be characterized by an apparent binding energy equal to the isoteric heat of adsorption of hydrogen on Fe-(100)-surfaces but with a coverage between that of an unstressed surface and between that of a deep trap in the bulk.

Résumé—Nous avons étudié la fragilisation de monocristaux de FeSi et de Ni par l'hydrogène, pour de faibles pressions d'hydrogène (10 mPa $\leqslant p\mathrm{H}_2 \leqslant$ 100 kPa). Nous avons utilisé une technique spéciale pour mesurer l'angle d'ouverture de l'extrêmité d'une fissure stable en cours de croissance en fonction de la température, de la pression d'hydrogène et de la vitesse. La relation entre α et la vitesse d'ouverture de l'extrêmité de la fissure dépend de la température. On peut distinguer trois domaines de températures: aux faibles températures (inférieures à 293 K) les phénomènes de transport contrôlent la fragilisation; aux températures intermédiaires (293 K $\leqslant T \leqslant$ 390 K) la fragilisation par l'hydrogène est contrôlée par la concentration en hydrogène à l'équilibre dans la zone de rupture et aux températures plus élevées la germination fragile de fissures devient difficile. Nous avons étudié en détail les phénomènes microscopiques qui se produisent au cours de la fragilisation par l'hydrogène à l'aide d'études au microscope électronique à balayage de la propagation *in situ* des fissures et par fractographie en MEB. Ces résultats, ainsi que l'étude de l'influence de mélanges oxygène–hydrogène sur le phénomène de rupture, àontrent que la rupture se produit à une distance de l'extrêmité de la fissure inférieure à 100 nm. Nous discutons des modèles de fragilisation par hydrogène qui relient cette fragilisation à une diminution de l'énergie superficielle, à une augmentation de la concentration en hydrogène dans la zone de rupture ou à la couverture de l'extrêmité de la fissure par l'hydrogène, et nous les comparons avec les résultats expérimentaux. Pour expliquer ces résultats, nous supposons que l'on peut relier la fragilisation par l'hydrogène à la couverture partielle d'un site spécial à l'extrêmité de la fissure sous contrainte. Avec cette hypothèse, les mesures de la variation d'α en fonction de $p\mathrm{H}_2$ et de T montre que ce site peut être caractérisé par une énergie de liaison apparente égale à la chaleur isostère d'absorption de l'hydrogène sur les surfaces Fe-(100), mais avec une couverture comprise entre celle d'une surface sans contrainte et celle d'un piège profond dans le cristal massif.

Zusammenfassung—Es wurde die Wasserstoffversprödung an FeSi- und Ni-Einkristallen bei sehr niedrigen Wasserstoffpartialdrücken (10 mPa $\leqslant p\mathrm{H}_2 \leqslant$ 100 kPa) untersucht. Eine spezielle Versuchstechnik ermöglicht die Messung des Rißöffnungswinkels α an einem stabil laufenden Riß als Funktion der Temperatur, des Wasserstoffpartialdrucks und der Rißöffnungsgeschwindigkeit. Mit dieser Technik kann man drei Temperaturbereiche unterscheiden, bei tiefen Temperaturen ($T \leqslant$ 293 K) wird die Versprödung durch die Nachlieferung des Wasserstoffs zur Brucheinflußzone bestimmt, in einem mittleren Temperaturbereich (293 K $\leqslant T \leqslant$ 390 K) läßt sich die Versprödung durch die Gleichgewichtskonzentration des Wasserstoffs in der Brucheinflußzone beschreiben und bei noch höheren Temperaturen ($T \geqslant$ 390 K) reicht die Spannung zur Bildung eines Spaltbruchs nicht mehr aus. Detaillierte fraktographische Untersuchungen des Bruchprozesses, *in situ* Zugversuche im Rastermikroskop und Messungen des Einflusses von Sauerstoffbeimengungen auf den Bruchprozeß zeigen, daß die Brucheinflußzone nicht mehr als 100 nm vor der Rißspitze liegen kann. Modelle, die die Wasserstoffversprödung entweder mit der

Änderung der Oberflächenenergie, mit der Zunahme der Wasserstoffkonzentration in der plastischen Zone oder mit der Wasserstoffbedeckung an der Rißspitze korrelieren, werden mit den Messungen verglichen. Zur Erklärung der Messergebnisse wird angenommen, daß sich die Wasserstoffversprödung durch die Besetzungszahlen eines speziellen Platzes an der Spitze eines belasteten Risses beschreiben läßt. Messungen der Druck- und Temperaturabhängigkeit von α ergeben dann, daß sich dieser Platz mit einer Bindungsenergie beschreiben läßt, die mit der isosteren Desorptionwärme des Wasserstoffs auf (100)-Fe-Oberflächen übereinstimmt. Die Besetzungszahlen dieses Platzes liegen hingegen zwischen den Besetzungszahlen spannungsfreier Oberflächen und denen tiefer Volumentraps.

INTRODUCTION

The fracture toughness of steels is strongly influenced by low pressure hydrogen gas [1, 2]. The various microstructures of steels complicate the modelling of the threshold (K_{thr}) behaviour as well as the description of the pressure and temperature dependence of the crack growth rate. In addition, depending on the purity of the alloy, co-segregation phenomena can favor or hinder intercrystalline crack growth [3, 4]. Most models relate the change in toughness K_{thr} to the surface energy γ which in turn depends on the interface considered and on the coverage θ of adsorbed hydrogen on this interface [5–7]. Other models relate the toughness change to the hydrogen concentration, c_H, at a critical distance from the crack tip [8, 9]. This concentration is controlled by the stress field in the plastic zone and by the type and number of traps in this zone. Hence all models predict a strong dependence of the toughness on γ or the hydrogen concentration. Even for a grain boundary the work of separation is not a state function but a function of the separation path [10]. However, for pure single crystals the microstructure is well known and problems arising from the presence of interfaces can be excluded.

Another interesting problem is to clarify how the change of the surface energy γ can influence hydrogen assisted crack growth in cases where plastic flow occurs and where the surface energy is an almost negligible contribution to the fracture energy. Thomson and others [5, 11, 12] assumed that the local crack tip region remains brittle and is screened from the applied stress by a surrounding dislocation cloud. For these conditions a small change in γ directly increases the crack driving force [11, 13]. FeSi single crystals, which can cleave even in vacuum, seem to be a possible material to study applications of these models [14].

The models discussed above assume local equilibrium of hydrogen at the crack tip. Frequently it seems that surface reactions control the brittle crack growth rate and that the amount of brittleness observed can be described by the pH_2 and T dependence of the coverage of adsorbed hydrogen at the crack tip [15–17]. Isotherms of hydrogen coverage as well as surface reaction rate constants are well known for Ni- and Fe-single crystal surfaces [18–20]. Therefore, measurements of hydrogen assisted crack growth in FeSi- and Ni-single crystals as a function of hydrogen pressure, temperature and displacement rate should reveal details of the fracture process and of the controlling rate process.

Single parameters like the stress intensity factor K or the J-integral often characterize the stress field near the crack tip. However, in single crystals, due to anisotropic plasticity, a single parameter like J does not describe correctly the stress amplitude. Even if J could be used the criteria of validity for J were violated for the small specimen sizes used in tests with single crystals [21]. But for suitably oriented single crystals the crack tip angle α can be used to characterize the amount of ductility accompanying crack growth. For ideal ductile crack growth this angle depends only on the slip geometry and on the coarseness of slip [22]. Crack tip angles α smaller than the angle α^d between the active slip lines are obtained only if an additional fracture process like local cleavage (Δa_i^H in Fig. 4) is observed. Therefore, the angle α will be applied throughout the paper as a quantitative measure of embrittlement.

Stable crack growth tests in tension and tension-compression were carried out in an ultra high vacuum chamber (10 nPa) at hydrogen pressures from 10 mPa to 100 kPa. In vacuum the crystals deform by general yield. This allows to prescribe the ductile crack growth rate between 10 nm/s and 100 μm/s. The object of the present work was to investigate the influence of the hydrogen concentration at the crack tip on the brittleness of fracture under steady state conditions (low crack growth rates) and the influence of the kinetics of crack growth for high growth rates at which surface reactions and transport processes become rate limiting.

EXPERIMENTAL

Fe–2.6%–Si single crystals and Ni-single crystals were tested in a closed loop hydraulic system in tension and in tension-compression. The specimen geometry is shown in Fig. 1. In order to produce plane fracture surfaces and straight crack fronts in b.c.c.- and f.c.c.-single crystals the same orientation (⟨100⟩-specimen axis, direction of the root of the notch ⟨110⟩) can be used but the active slip systems are different for FeSi ({112} ⟨111⟩) and for Ni ({111} ⟨110⟩) [23, 22]. Prior to testing all specimens were pre-cracked in low cycle fatigue at a hydrogen pressure of 100 kPa. In order to detect hydrogen embrittlement in Ni single crystals (yield strength 25 MPa) a high yield stress is required. Therefore the unnotched Ni-specimens were cyclically hardened in

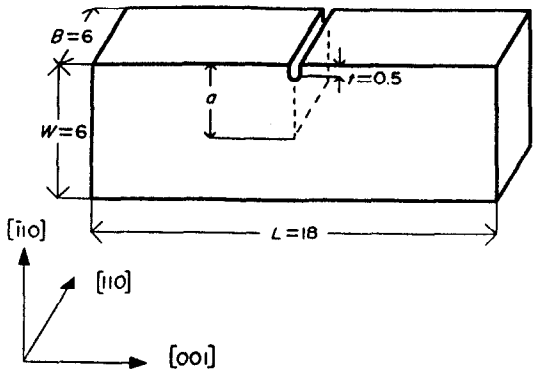

Fig. 1. Specimen geometry for the FeSi and Ni single crystals. Orientation: ⟨001⟩ specimen axis and {110} specimen surfaces (dimensions in mm).

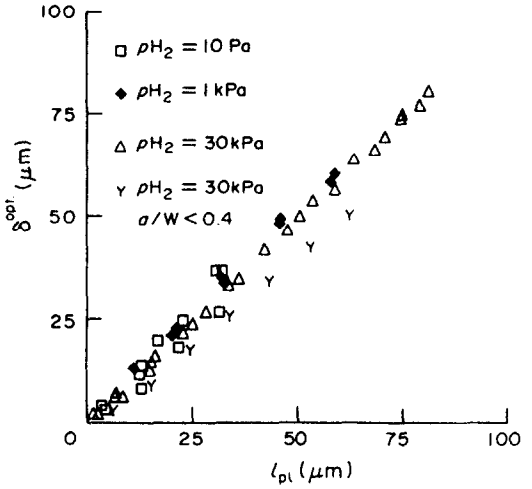

Fig. 2. The crack tip opening δ^{opt}, measured optically, as a function of the plastic elongation l_{pl} for different hydrogen pressures pH_2 and crack lengths a.

vacuum by linearly increasing the stress amplitude from zero to 128 MPa in 60,000 cycles.

For the orientations described above the crack grows in vacuum by alternating slip with a constant crack tip opening angle, α, [23]. In hydrogen this angle decreases with increasing hydrogen pressure. The decrease in angle is measured by the following procedure: pre-cracked specimens are loaded in tension and after a constant plastic elongation increment Δl_{pl}, the specimen is unloaded in order to produce markings on the fracture surface (Fig. 8). The distance of these unloading lines characterizes the crack advance Δa per increment Δl_{pl}. The dependence of the crack opening δ on l_{pl} is measured optically for various hydrogen pressures. For crack lengths, a, smaller than 0.4 W, where W is the specimens width, work-hardening as well as deviations from the linear relationship between δ and l_{pl} are observed (Figs 2 and 3). For crack lengths greater than 0.4 W the plastic elongation, l_{pl}, is found to be equal to δ (Fig. 2). In this range the net stress $\sigma_{net} = P/(W-a)B$, where P is applied load and B the specimen thickness (Fig. 1), remains constant (Fig. 3), indicating fully plastic conditions. Both results indicate, that all the slip activity emanates from the crack tip and traverses all the ligament. Thus for $a/W \geqslant 0.4$, δ may be measured via l_{pl}.

All tests are controlled by a mini-computer (DEC LSI 11). During unloading up to 400 force-elongation (P_i, $l_{t,i}$, $1 \leqslant i \leqslant 400$) values are measured and stored. From these data the compliance, C, and the plastic elongation Δl_{pl} are computed on-line by linear regression, $l_{t,i} = \Delta l_{pl} + CP_i$. Together with the crack growth data the ratio $a_n = 2\Delta a/\Delta\delta$, which is directly related to the crack tip angle [$a_n = \cot(\alpha/2)$, see Fig. 4] can be calculated. In this way the crack tip angle was obtained as a function of hydrogen pressure and temperature.

Repetitive unloading of the specimen, which is necessary for the compliance measurement, does not interfere with crack propagation. This was tested by varying the lower reversal point from zero load to 0.9 P_{max}.

Prior to every change of the hydrogen pressure the crack was resharpened by three loading cycles with high pressure hydrogen gas ($pH_2 = 30$ kPa). Thereafter the specimen chamber was evacuated and then the new test pressure was applied.

Each data point in the following figures is the average of more than five a_n-measurements from at least two specimens.

The experimental equipment is shown schematically in Fig. 5. The experiments were carried out in a UHV stainless steel chamber. A pressure of 10 nPa can be attained after degassing the entire system. After pre-cracking and after every pressure change the chamber is evacuated by the integrated ion getter pumps (IGP) to pressures of less than 10 μPa. Then hydrogen gas (purity 99.999%) passing a gas purifier (Oxisorb) (O_2T) and a liquid nitrogen trap (LN_2) is filled via the valve V1 into the chamber (CH1). The partial pressure of hydrogen and of the residual gases is measured by a quadrupol mass

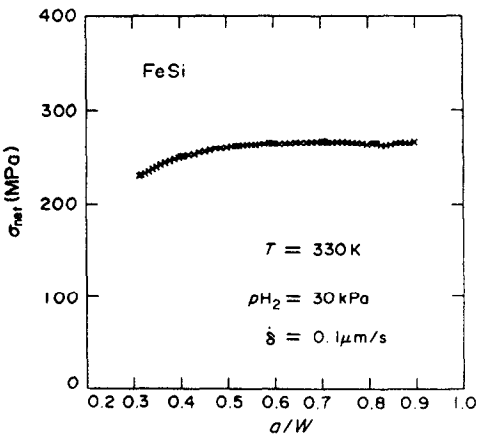

Fig. 3. Dependence of the net stress $\sigma_{net} = P/(W-a)B$ on crack length a. P is the applied load, W the specimen width and B the specimen thickness.

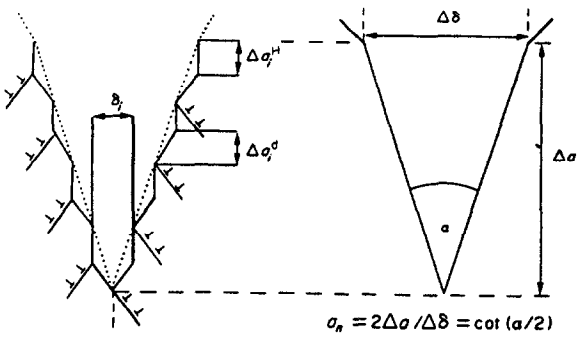

Fig. 4. Schematic drawing of a crack tip produced by micro cleavage and alternate slip. $\Delta\delta$ is the increase in crack opening after an increase of crack length Δa. Δa_i^H and Δa_i^d are the microscopic growth steps produced either by hydrogen induced cleavage or by ductile rupture.

spectrometer (Balzers QMG 111) (QMS). Depending on the pressure used the gas purity is controlled in the specimen chamber ($pH_2 \leqslant 10$ mPa) or in a separate vacuum chamber (CH2) ($pH_2 \geqslant 10$ mPa). CH2 is connected with the specimen chamber via a valve (V2) with a constant calibrated leak rate. This allows to maintain a reduced pressure in CH2 for the operation of the quadrupole mass spectrometer (QMS).

For pressures of less than 10 Pa the hydrogen gas contaminates due to surface reactions at the walls of the chambers. Thus an appropriate flux of hydrogen gas through the specimen chamber was maintained by a separate pumping unit (flux through V3) in order to limit residual impurity concentrations to less than 0.1%.

The pressure is measured by an ion gauge (Leybold IM 110) (IG) for the low pressure region ($100\,\mu Pa \leqslant pH_2 \leqslant 100$ Pa) and by a total pressure meter (Balzers APG 010) (APG) for the high pressure region ($100\ Pa \leqslant pH_2 \leqslant 0.1$ MPa). Molecular pumps (TP) are used in addition to diffusion pumps (DP) in order to reduce the hydrocarbon contamination from the pumping oil. Under these purity conditions hydrogen embrittlement could be detected at pressures as low as 10 mPa.

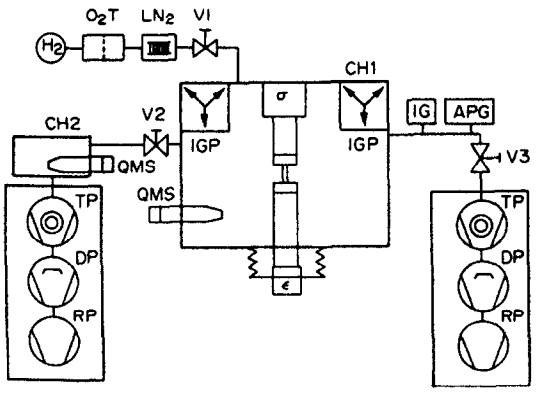

Fig. 5. Schematic drawing of the experimental equipment. The abbreviations are explained in the text.

For temperatures above room temperature the specimen as well as the walls of the specimen chamber are kept at the same temperature in order to obtain thermal equilibrium. This is important for pressures, at which the mean free path is of the order of the chamber dimensions ($pH_2 \leqslant 1$ Pa). The temperature is controlled by the mini-computer with an accuracy of 0.5 K. Temperatures down to 220 K can be reached by indirect cooling of the specimens with cold nitrogen gas.

RESULTS

Figure 6 shows three typical crack tips as they appear on the side faces of the specimens. The micrographs demonstrate the dependence of the crack tip angle on hydrogen pressure under otherwise constant conditions. In the following we shall discuss some results, which demonstrate the connection between the crack tip angle and topographical features of the fracture planes.

Figure 7 shows six photographs of a (100)-fracture surface, which were taken after crack growth at various hydrogen pressures. At constant temperature the surface roughness increases with decreasing hydrogen pressure (upper row of Fig. 7). At constant pressure the same is observed with increasing temperature (not shown in Fig. 7). Thus neither temperature nor hydrogen pressure alone control the appearance of the fracture surfaces. But, whenever the crack tip angle α is the same, even at different pressures and temperatures, similar patterns are observed on the fracture surfaces (lower row of photographs in Fig. 7). This shows that α characterizes the topographic details of the fracture surfaces and supports the view, that α is a useful local measure for the ductility of the fracture process.

Since the fracture surfaces are far from being flat at a typical SEM magnification, the question arises, whether the crack tip opening angle which is determined by macroscopic measurements has any local relevance at the scale of Fig. 7. It is very unlikely that

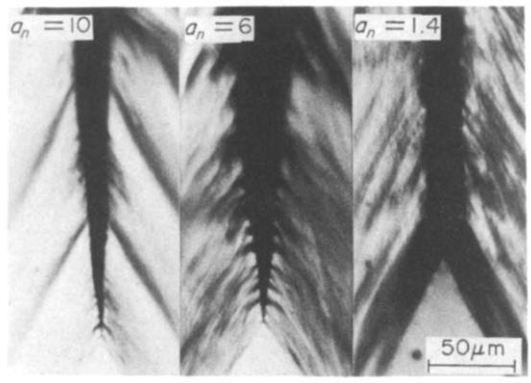

Fig. 6. Optical photographs of the crack tip obtained after straining at different hydrogen pressures (10 Pa, 0.7 Pa, vacuum). The viewing direction is ⟨100⟩, temperature: 300 K, $\dot{\delta} = 100$ nm/s.

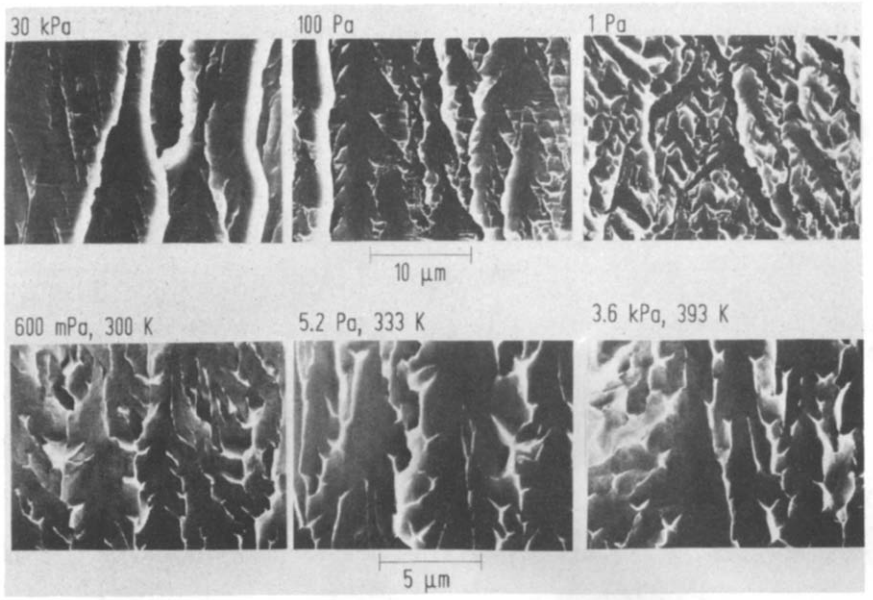

Fig. 7. (100) fracture surfaces of a FeSi single crystal taken after stable tensile crack growth in different hydrogen atmospheres. The upper row demonstrates the influence of pressure on the microstructure, the lower row shows that at different pressures and temperatures the same microstructural features are found, if the crack tip angle α ($\alpha = 20°$) is the same (crack growth direction from top to bottom).

the crack tip angles remain constant, when the crack tip moves across the topography, which is shown in Fig. 7. In order to reveal more details of the behaviour of the crack tip angle on such a microscopic scale the following observations are helpful: the fracture surface consists of rather flat areas and acute elevations, which resemble a pyramid with triangular base (Fig. 7, upper row, photograph 2). Observations of many fracture surfaces show, that these pyramids are isolated and are surrounded by the flat areas of the fracture surface. (See also Fig. 7.) If the flat areas are followed along the direction of the crack propagation no steps are encountered over long distances. Only river-pattern-like steps, which run more or less parallel to the crack propagation direction, are found. Thus the mixture between ductile rupture and genuine fracture (as indicated in Fig. 4) must happen on a finer scale, which is not resolved in Fig. 7. Therefore the measured crack tip angle must be that of the local crack tip, when it produces the flat areas of the fracture surfaces. The pyramids are obviously enclaves, which were left behind by the crack tip and are necking down in a ductile manner to a chisel point after the main crack front has moved forward. This tendency to ideal ductile slide off processes becomes more pronounced with increasing ductility (i.e. larger crack tip angle on the flat areas).

In some respects the topology of the crack front observed here is similar and opposite to that of dimple fracture. In the latter case there is continuous crack front and *ahead* of the crack front there are holes, i.e. isolated pieces of crack front, which grow and join the approaching continuous crack front. In our case there is a continous crack front, which leaves *behind* enclaves of yet unseparated material, which neck down in an ideal ductile manner.

These conclusions are supported by *in situ* observations in a SEM. In our experiments hydrogen

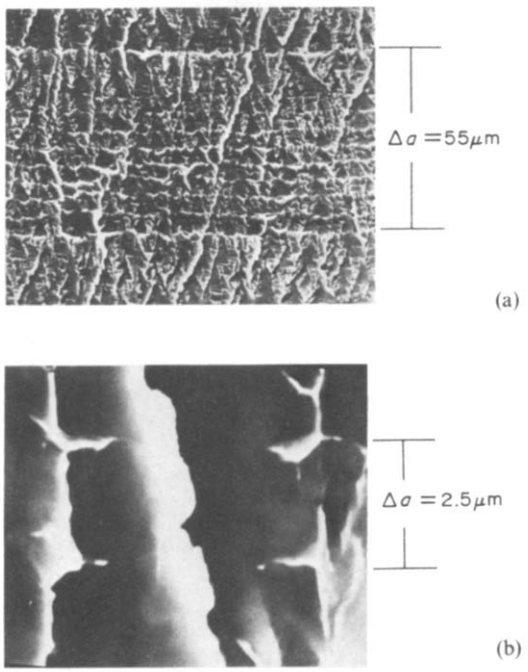

Fig. 8. (a,b) Unloading markings on a (100)-fracture surface. A high magnification of two unloading markings (specimen unloaded to 0.9 P_{max}) obtained after a controlled plastic elongation increment of 250 nm ($a_n = 10$, $\Delta a = 2.5\,\mu$m).

embrittlement can already be observed at hydrogen pressures (≥ 10 mPa) low enough to maintain a proper SEM image. The straining inside the scanning electron microscope was done by means of a tensile stage, which is described elsewhere [23]. In these tests the crack front can be observed during propagation. In this way it was observed *in situ* that isolated micro-cracks initiate along the crack front and encircle the uncracked material between the micro-cracks. The resulting plastic enclaves continued to neck down to zero cross-section, while the crack front continued to propagate far ahead.

The preceding results may be summarized in the following way: The plastic bridges are responsible for the roughness of the fracture surfaces, but are of no relevance for the crack tip angle, since α is determined from markings on the flat areas. Thus the measured value of α is the value of the crack tip angle during the formation of the flat areas. From the roughness of these areas, which is barely visible at the resolution of the SEM, it can be concluded, that α is a meaningful quantity down to a scale of 0.1 μm. This means, that the mixture of plastic shearing off processes and cleavage-like decohesion processes (Fig. 4a), which is responsible for the value of α, happens on a scale of 0.1μm or less.

Several direct tests were carried out to examine the stability of the crack. By partial unloading markings can be produced on the fracture surfaces as is demonstrated in Fig. 8(a). During reloading the crack becomes locally ductile again as described above (white markings perpendicular to the direction of crack propagation in Fig. 8). Plastic elongation increments Δl_{pl}, of approximately 100 nm can be produced by our technique. This yields crack growth increments of 0.5 μm for $a_n = 10$. Markings produced after plastic elongation increments of 250 nm are shown in Fig. 8b. The local a_n values obtained from the distance of these markings correspond to the a_n values obtained with larger increments. This is direct experimental evidence that the crack grows without discontinuous jumps down to a scale of less than 1 μm.

In our experiments with low pressure hydrogen gas the question arises whether the transport of hydrogen to the fracture process zone is a rate limiting step or not. In order to clarify this question the normalized crack growth rate was measured for various crack growth rates $\dot{a}$. The crack growth rate $\dot{a}$ is obtained from the prescribed δ and a_n via $\dot{a} = a_n \dot{\delta}/2$. Figure 9(a) shows the results of a typical test on FeSi single crystals. The variation a_n with $\dot{a}$ is less than the experimental scatter whereas the pressure dependence of a_n can be resolved clearly. Nickel shows a similar behaviour above room temperature (Fig. 9(c) and [24]). Since α does not depend on the crack growth rate hydrogen transport processes to the crack tip are not rate limiting. Thus, at these crack growth rates (100 nm/s $\leq \dot{a} \leq$ 100 μm/s) and at temperatures between 273 and 373 K (for FeSi) the hydrogen concentration near the crack tip must be in local equilibrium with the gas phase.

Below room temperature a_n decreases in nickel with increasing crack growth rate (Fig. 9c). This

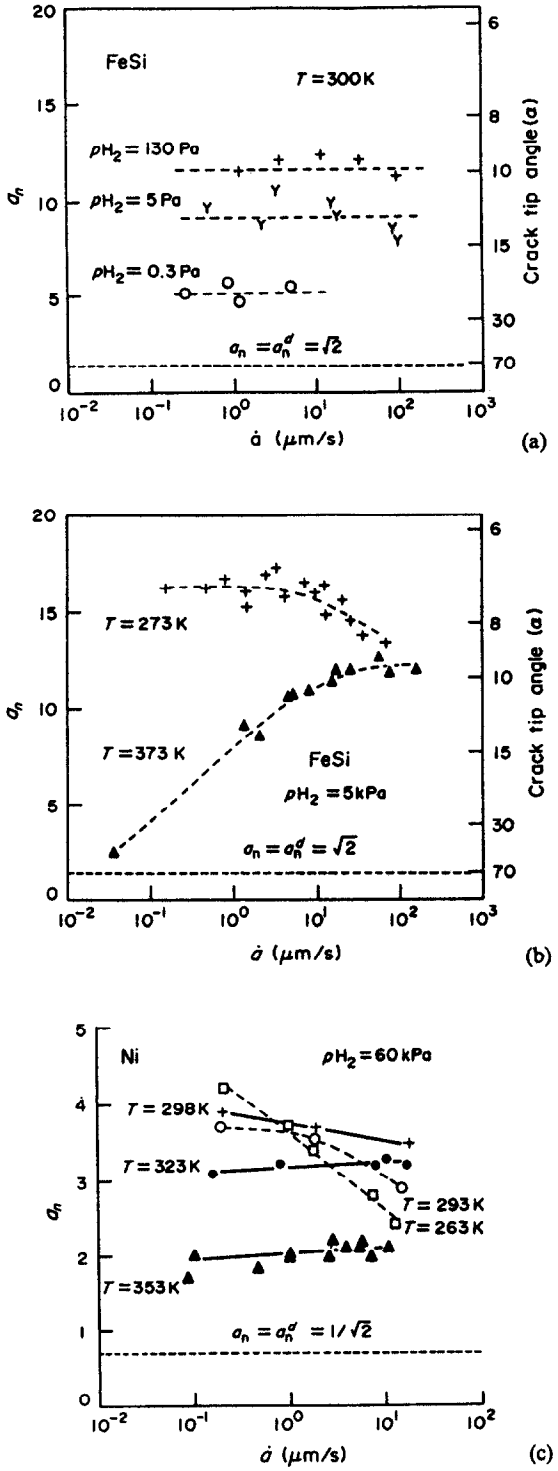

Fig. 9. (a,b,c) Influence of the crack growth rate $\dot{a}$ on the normalized rate $a_n = \cot \alpha/2 = 2\dot{a}/\dot{\delta}$ for different hydrogen pressures and temperatures (FeSi). $\dot{a}$ is controlled via $\dot{\delta}$. The dashed lines are spline fits. (c) The same for Ni for different temperatures.

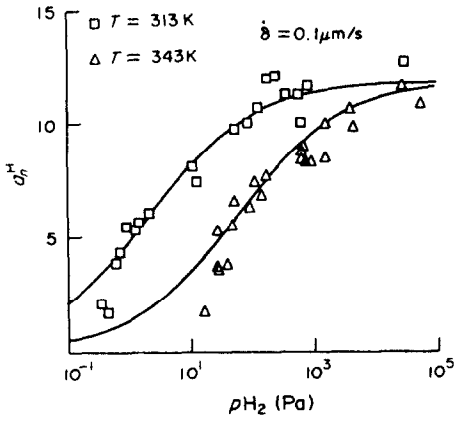

Fig. 10. a_n^H as a function of hydrogen pressure pH_2. The sigmoidal curves are obtained from equation (2) with U, K_0 and β from Table 1.

result, which contrasts the observations of Kamdar [25], demonstrates, that transport processes to the fracture process zones become rate limiting. FeSi seems to show the same trend (Fig. 9b) but the crystals tend to cleave catastrophically at low temperatures ($T \leqslant 273$ K) and high crack growth rates, which limits the experimentally accessible range. Above 373 K, a_n decreases with decreasing rate and for the lowest rates no embrittlement is observed (Fig. 9b) because hydrogen embrittlement depends on yield strength [3] which is rather low under these conditions (see discussion).

All the following results were obtained under conditions for which hydrogen equilibrium may be assumed because the crack tip angle is independent of the crack growth rate.

In order to be able to relate hydrogen embrittlement to other measurable quantities, we need a quantitative measure for this important effect. For this purpose we reconsider Fig. 4 and note, that the crack growth is the sum of two contributions: the ideally ductile increments, Δa_i^d, and ideally brittle fracture increments without plasticity, Δa_i^H

$$\Delta a_i = \Delta a_i^d + \Delta a_i^H.$$

Dividing by $\delta_i/2$ yields

$$a_n = a_n^d + a_n^H \qquad (1)$$

with $a_n^d = \cot(\alpha^d/2)$, where α^d is the angle between the two slip planes involved [26]. Obviously, $a_n^H = 0$ characterizes ideal ductile fracture and $a_n^H \geqslant 0$ is a quantitative measure of the embrittlement.

Figure 10 shows a typical plot of a_n^H vs $\log pH_2$ ($\dot{\delta} = 0.1\ \mu$m/s) for two temperatures. The measurements cover a range of six orders of magnitude in pressure. The gas purity used in our experiments allows to distinguish hydrogen assisted crack growth from ductile crack growth ($a_n^H = 0$) down to pressures of 10 mPa. At higher pressures the a_n^H values seem to saturate, since a_n^H does not change markedly over two orders in magnitude of pressure (Fig. 10, $T = 313$ K). Measurements of this kind were reported in a previous work [27] but the results shown below are achieved with an improved technique and cover a greater range of pressures and temperatures.

A careful study of the pressure and temperature dependence of a_n^H yields that the relationship

$$X/(1-X) = k_0 \cdot \sqrt{pH_2} \cdot \exp(U/kT);\ X = a_n^H/\beta \qquad (2)$$

gives the best fit to the data. The constants β, U and k_0 were obtained in the following ways:

In order to determine β, equation (2) is transformed to

$$1/a_n^H = (1/\beta)\{[\exp(-U/kT)/k_0\sqrt{pH_2}] + 1\} \qquad (3)$$

showing that β is the saturation value of a_n^H for large pressures. Plotting $1/a_n^H$ against $1/\sqrt{pH_2}$ should yield straight lines. β is determined from the intersection of these lines with the ordinate ($pH_2 = \infty$). A value for

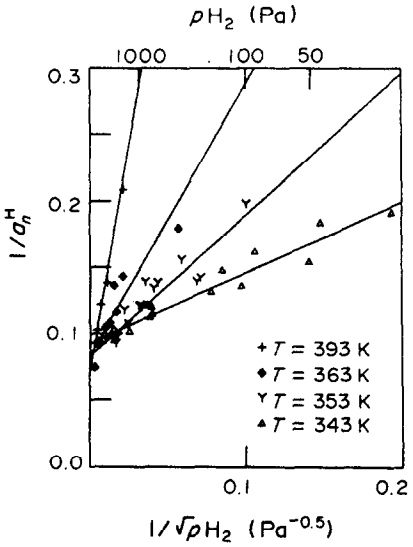

(a)

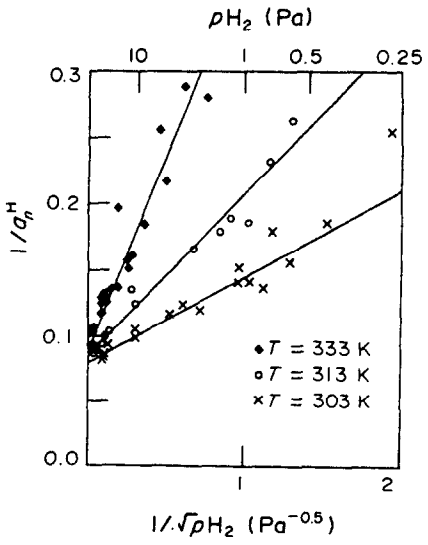

(b)

Fig. 11. (a,b) $1/a_n^H$ vs $1/pH_2$ for different temperatures. The straight lines are fitted from equation (3).

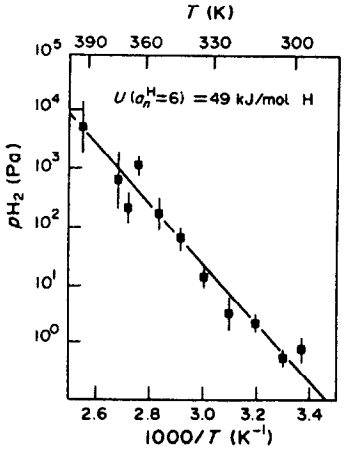

Fig. 12. The hydrogen pressures, which yield a constant a_n^H value, as a function of temperature. The data points are calculated from fits as given in Fig. 11(a,b). The straight line is fitted from equation (2) for $a_n^H = 6$.

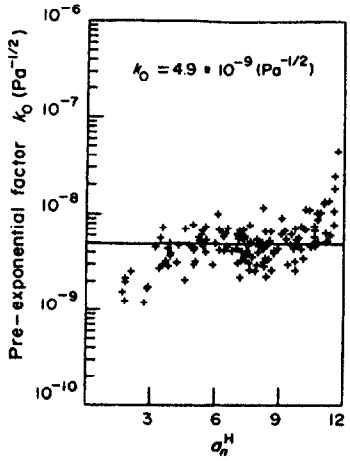

Fig. 13. The pre-exponential term, k_0, from equation (2) as a function of a_n^H. The points are calculated from all data with equation (F2) and β, U from Figs 11 and 12. The straight line is a least square fit through the data.

β of 11.8 ± 0.2 is obtained. This is demonstrated in Fig. 11(a,b) for several temperatures, β is found to be independent of pressure and temperature in the ranges examined.

U is obtained from Arrhenius plots of $\log(pH_2)$ against $1/T$. According to equation (2) straight lines should be obtained for $a_n^H = \text{const}$. Figure 12 shows an example. Their slopes yield $U = 49$ kJ/mol H.

Finally, the pre-exponential factor k_0 is obtained by solving equation (2) for k_0 and calculating all possible values of k_0 from the experimental data and the values of β and U just obtained. Figure 13 shows these values of k_0 plotted vs a_n^H. The data cover a temperature range from 273 to 400 K and a pressure range from 10 mPa to 0.1 mPa. The pre-exponential factor k_0 in Table 1 was obtained from this plot by a least square fit. The two sigmoidal curves given in Fig. 10 were obtained from equation (2) using the values of β, U and k_0 given above.

Figure 13 gives a visual impression of the quality of the fit according to equation (2) in comparison with the experimental scatter, because all data are combined in one plot. The fit is good for $4 \leqslant a_n^H \leqslant 11$. The deviations of k_0 for the largest a_n^H-values reflect the fact that deviations from ideal saturation behaviour of $a_n^H(pH_2)$ is observed at the highest pressures used in our experiments.

During tests at low growth rates ($\dot{a} \leqslant 150$ nm/s) and at low pressures ($pH_2 = 1$ Pa) a known amount of oxygen was expanded into the specimen chamber. The load necessary to propagate the crack stops decreasing within a second which corresponds to a 30 nm crack opening displacement (Fig. 14c) and the a_n value decreases (indicated dark area in Fig. 14a). From these tests a fracture process zone size of less than 150 nm can be estimated (see Discussion).

DISCUSSION

A microscopic theory describing the influence of an aggressive environment on stable crack growth is still lacking. The existing models only impose thermodynamic restrictions on the quasi-static growth of cracks. Because of this situation we start from the experimental observations and try to develop a consistent picture based upon the experimental results. Subsequently, we summarize the results which must be incorporated in a microscopic theory.

The experiments show that in gaseous hydrogen stable crack growth with a constant crack tip opening

Table 1. The apparent binding energy U and the pre-exponential factor k_0 [equation (2)] for the fractional coverage of deep volume traps n, for the surface coverage θ and for the normalized crack growth rate a_n^H/β

Curve in Fig. 16	X	k_0 ($Pa^{-1/2}$)	U (kJ/molH)	Reference
1	n	$2.8 \cdot 10^{-7}$	32.7	42
2	n	$1.87 \cdot 10^{-6}$	26	43
3	θ	$2.18 \cdot 10^{-5}$	41	45
4	θ	$7.6 \cdot 10^{-7}$	50.2	18
5	θ	$3.8 \cdot 10^{-6}$	43.3	19
6	θ	$8.5 \cdot 10^{-7}$	30	19
Data points	$(H_2 + O_2)$ a_n^H/β	$4.9 \cdot 10^{-9}$	48.8	Present

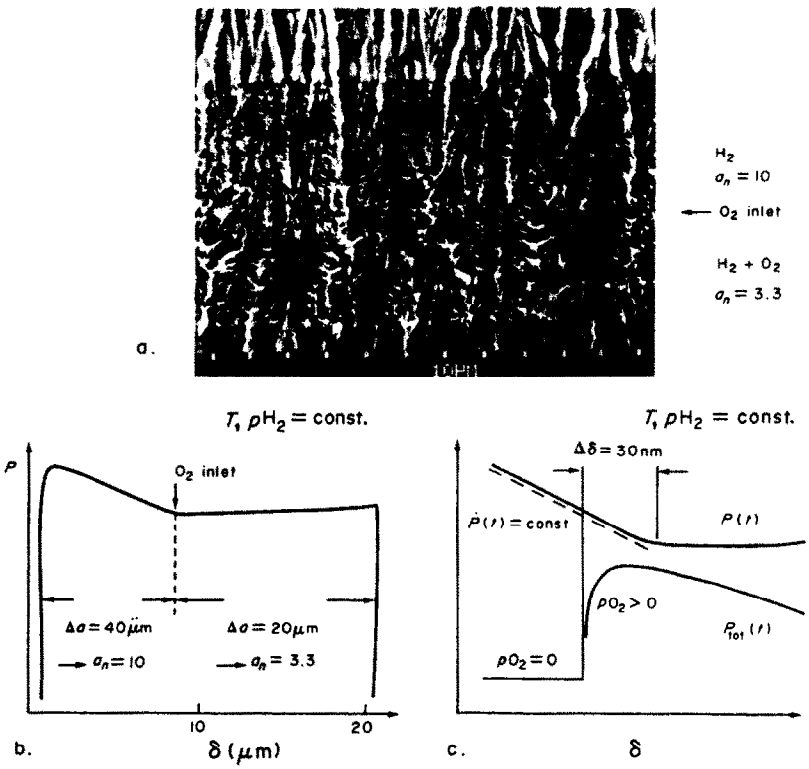

Fig. 14. (a) (100) fracture surface, upper bright region $pH_2 = 1$ Pa, lower darker region $pH_2 = 1$ Pa, $pO_2 = 1$ Pa, a_n decreases due to O_2 inlet, $T = 300$ K. (b) Force-elongation curve obtained from this test, the load P stops decreasing after O_2 inlet. (c) Magnified view of the force elongation curve (Fig. 14b) together with $p_{tot} = pH_2 + pO_2$ as recorded by a pirani pressure meter ($\dot{\delta} = 30$ nm/s).

angle α can be obtained. During stable growth the nominal stress σ_{net} remains constant in hydrogen (Fig. 3). Therefore even in the hydrogen environment the cracks grow under fully plastic conditions.

In addition, the plastic elongation amplitude, l_{pl} corresponds to the plastic crack tip opening δ ($l_{pl} = \delta$) showing that all plastic strain emanates from the crack tip and opens the crack (Fig. 2) (this allows to control δ via l_{pl} experimentally). McClintock [28] has examined this case using slip-line-theory. In the framework of this theory he finds that crack tip angles smaller than the angle between the two slip planes involved, α^d, can only be obtained, if another fracture mechanism, which yields zero crack tip angles, is superimposed with some crack growth rate c (in Fig. 4: $c = \Delta a_i^H/\Delta t_i$, Δt_i is the time between increments). Such fracture mechanisms may be local micro-cleavage or void formation. With this assumption he finds for the crack tip opening angle of a stable growing crack in an nonwork-hardening solid with $\alpha^d = 90°$ $\tan\alpha/2 = \dot{\delta}/(\dot{\delta} + 2c)$. For general slip plane configurations characterized by $a_n^d = \cot(\alpha^d/2)$ the equation becomes $\tan\alpha/2 = \dot{\delta}/(\dot{\delta}a_n^d + 2c)$. Together with equation (1) and $a_n = \cot(\alpha/2)$ we get $c = a_n^H\dot{\delta}/2$, which amplifies, that a_n^H characterizes the hydrogen induced crack growth per plastic crack opening.

It is important to know, whether the mixture between plastic blunting (a_n^d) and cracking (c or a_n^H) as indicated by Fig. 4 happens on an atomistic scale (emission of isolated dislocations mixed with breaking isolated rows of atomic bonds) or on a macroscopic scale (brittle discontinuous macroscopic crack jumps followed by extensive plastic blunting) or on an intermediate scale. From the regularity of markings produced by unloading, it must be concluded that possible discontinuous growth steps are smaller than 1 μm for $a_n = 10$ (local opening $\Delta\delta = 200$ nm). This upper limit can be reduced further by direct inspection of the fracture surfaces: It was shown that the smooth areas are *not* ideal cleavage facets but are areas, where the crack tip angle has the measured value ($8° \leqslant \alpha \leqslant 30°$). Therefore the steps Δa_i^H from Fig. 4 should be visible on these areas. From the resolution of the SEM it can thus be concluded that the Δa_i^H are smaller than 0.1 μm.

Which fracture mechanism produces the $\Delta a^H{}_i$? According to the present knowledge in single crystals only micro-cleavage or void formation ahead of the current crack tip (Lynch [29]) are possible candidates.

Examinations of the fracture surface inside a scanning electron microscope show no evidence of micro-dimples. Some specimens were sent to S. P. Lynch to repeat our experiments and to examine the fracture surface with his replica technique. He also found no clear evidence for micro-dimples [30]. Furthermore in

gaseous hydrogen the fracture surfaces always coincide locally with the cleavage surface ({100} for FeSi) even for cases were this surface is inclined up to 90° to the tension axis (Fig. 15). Figure 15 shows a {110} fracture surface with secondary cracks on the {100} plane (specimen axis ⟨110⟩). In vacuum these cracks can stop (upper middle part of Fig. 15) whereas in hydrogen new cracks on the {100} surface form (middle part of Fig. 15). There is no reason why voids should form preferentially along {100} planes. Therefore the micro-void mechanism can be excluded for pure FeSi single crystals.

If the mechanism is micro-cleavage, it is important to know, whether cleavage occurs at the crack tip, just extending the existent crack, or whether cleavage crack initiation occurs ahead of the crack tip due to the high hydrostatic tension in front of the tip [31]. Since the cleavage is enhanced by hydrogen coming from the gas phase, the different positions of the cleavage process may in principle be distinguished by the kinetics of the hydrogen transport: cleavage as an extension of the existing crack tip is most likely influenced directly by the coverage of adsorbed hydrogen at the crack tip, whereas the initiation of micro-cracks ahead of the crack front requires diffusion of hydrogen into the bulk. However, the diffusivity of hydrogen in Fe–Si single crystals is high ($D_{FeSi} = 2.8 \cdot 10^{-4} \exp[-4.3/RT(\text{kJ/mol})]$ (cm²/s) [32]. Hydrogen can diffuse several micrometers inside the bulk for all crack growth rates used in our tests. Therefore, from hydrogen diffusivity alone we are not able to distinguish between bulk and surface effects. In Ni at room temperature the diffusivity of hydrogen $\{(D_{Ni} = 4.2 \cdot 10^{-3} \exp[-39.3/\text{RT(kJ/mol)}]$ (cm²/s) [33]} is five orders of magnitude lower than in FeSi. For the high pressures and temperatures used in our tests (Fig. 9c) hydrogen transport through the gas phase and the surface reaction rates are always fast enough [20]. Therefore it is believed that hydrogen transport through the bulk to the fracture process zone (FPZ) limits the crack growth rate. From the diffusivity D_{Ni} and from the decrease of a_n with increasing $\dot{a}$ ($\dot{a} = 1\ \mu$m/s, $T = 293$ K, Fig. 9c) the FPZ is estimated to lie approximately 10 nm from the tip [34]. This value is a lower bound since the effective diffusivity can be several orders of magnitude higher due to dislocation transport [35]. For the higher crack growth rates $\dot{a}$ the dislocations can break away from their hydrogen atmosphere [36] and this transport mechanism ceases to be effective which likewise yields a decrease in a_n with increasing $\dot{a}$. Therefore, even for Ni we are not able to distinguish between surface and bulk effects from diffusivity alone.

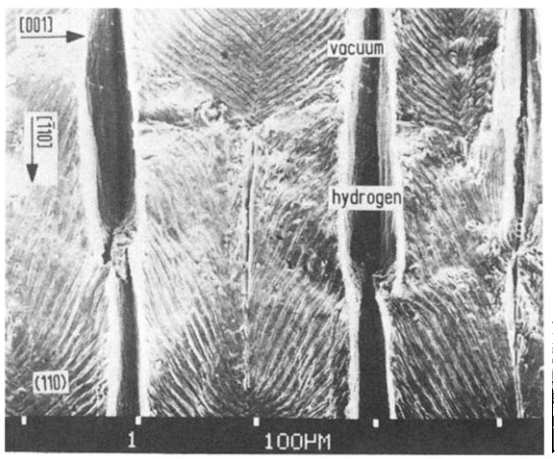

Fig. 15. (110)-fracture surface, showing that in an hydrogen environment cracks propagate along (001) even in cases where the (001)-planes are parallel to the loading direction.

In order to distinguish experimentally between the effect of adsorbed hydrogen and between hydrogen in the bulk, it is necessary to change one concentration without disturbing the other. In spite of the high diffusivity of hydrogen in FeSi this can be achieved with the help of oxygen: it is well known that oxygen replaces adsorbed hydrogen on (100) iron surfaces very efficiently [19]: by a partial pressure of oxygen equal to the partial pressure of hydrogen, the coverage of hydrogen can be reduced by four orders of magnitude. The point is, however, that no chemical reactions take place at room temperature between oxygen and hydrogen neither on the surface nor in the gas phase. Thus the chemical potential of hydrogen is unchanged. Therefore, in equilibrium the chemical potential of hydrogen in the bulk must remain constant. In addition, the concentration of hydrogen in all possible traps in the bulk is unchanged, because oxygen cannot enter the bulk due to its low solubility and diffusivity $\{D_0 = 3.7 \cdot 10^{-2} \exp[-42.3/RT(\text{kJ/mol})]$ (cm²/s) [37]} and thus cannot replace hydrogen. Thus oxygen hydrogen mixtures are the ideal means to change the surface coverage of hydrogen, while the bulk concentration of hydrogen remains unchanged under equilibrium conditions.

Of course, the assumption that equilibrium must be maintained is very restrictive. We tried to comply with it in two ways:

(1) We performed the tests at a low crack tip opening rate ($\dot{\delta} = 30$ nm/s), which is about thousand times lower than the rates at which rate effects become visible without oxygen at the same hydrogen pressures (1 Pa).

(2) We did not perform *continuous* crack growth experiments under hydrogen oxygen mixtures, but observed the change in crack growth behaviour, when the oxygen pressure was applied discontinuously during crack growth under hydrogen. Under these conditions the crack tip area is saturated with hydrogen at the moment when the oxygen pressure is applied, independent of what happens to the hydrogen transport afterwards.

In such experiments it is observed, that the fracture mode changes from $a_n = 10$ to $a_n = 3.3$ within a

second after the oxygen pressure is applied. Within this time the crack can propagate at most $10 \times 15\,\text{nm} = 150\,\text{nm}$, more likely is a value of $\sim 50\,\text{nm}$ (since a_n decreases within this time). Then the crack is nearly ductile, although the crack tip is still in the region of the bulk (several μm diameter), which is definitely saturated with hydrogen. From this result it must be concluded that the coverage of adsorbed hydrogen and not the presence of hydrogen in the bulk is a necessary requirement for hydrogen embrittlement.

This result is not surprising, if one reconsiders the locations at which hydrogen is present, though locally, in large enough concentrations for a significant reduction of cohesive forces: In the bulk the most abundant hydrogen traps are dislocation cores. Thus only one-dimensional *lines* of high concentration $c_H \cong 1$ are present in the bulk. On the average this does not raise the bulk concentration by any appreciable amount: detailed calculations of Hirth and Carnahan [38] show that a dislocation density of $1 \times 10^{15}\,\text{m}^{-2}$ loaded with hydrogen yields an enhancement factor of only 6 inside a cylindrical section of radius R, where R is the mean distance of dislocations. At the tip of a mechanically loaded elastic crack the same authors obtained a local concentration of 1 up to a distance of only 0.1 nm from the tip. If slow crack propagation is considered and if it is assumed that hydrogen is required at the very crack tip for hydrogen enhanced fracture, a continuous flux of hydrogen to the crack tip is required in order to maintain the equilibrium concentration at the crack tip. The tip is in immediate contact with the fracture surface, where on a two-dimensional area local hydrogen concentrations of the order of one are present, whenever the coverage approaches unity. Furthermore, hydrogen is highly mobile on the surface due to the low activation energy of surface diffusion [39]. Therefore, it seems very realistic to assume, that the surface is by far the most efficient reservoir for the required amounts of hydrogen. If this reservoir is blocked by oxygen, the embrittling effect ceases immediately, as found experimentally.

This leads to the following qualitative picture of the effect of hydrogen on the fracture process. In vacuum, at low rates the crack tip always blunts by the emission of dislocations whereas in hydrogen the probability of bond breaking versus dislocation emission is shifted towards bond breaking, because hydrogen is always present in high local concentrations at the very crack tip due to the efficient supply from the fracture surfaces and hydrogen reduces the cohesion forces (Oriani and Josephic [9]). Rice and Thomson [40] examined the balance between dislocation emission and bond breaking in a continuum approach by considering the forces which act on a dislocation near a crack tip. If the force on the dislocation due to the applied load outweighs the image and ledge forces which tend to pull the dislocation back into the crack even at atomic distances from the tip, spontaneous dislocation generation is assumed. The calculations show that the activation energy U_D for the brittle to ductile transition increases if the surface energy γ decreases due to the action of the environment. Thus the embrittling effects of hydrogen gas enter the theory only via a reduction of the surface energy. However, in this kind of approach it is difficult to explain, why other gases (i.e. oxygen), which adsorb as well as hydrogen, do not embrittle. Though, this is an old argument [41], it is still a valid one. Here we want to discuss another objection.

We observed experimentally, that embrittlement saturates with increasing hydrogen pressure at $a_n^H = 11.8$, i.e. well below ideal brittle behaviour. Increasing the hydrogen pressure by three orders of magnitude does not significantly change a_n^H (Fig. 10). However, the reduction of surface energy due to the adsorption of hydrogen does not saturate, which can be shown as follows: the dissociative adsorption of hydrogen obeys a Langmuir relationship [18, 19] of the following form

$$\theta/(1-\theta) = k_0 \sqrt{p} \cdot \exp(H_s/2kT) = \sqrt{ap} \qquad (4)$$

where k_0' is only weakly temperature dependent and H_s is the isosteric heat of adsorption. Describing the decrease of the surface energy γ with Gibb's equation yields

$$\gamma = \gamma_0 - \int \theta(\mu')\,d\mu' = \gamma_0 - (kT/b_0^2)\ln(1+\sqrt{ap}) \qquad (5)$$

where b_0 is the lattice constant, therefore, γ decreases continuously with increasing pressure [5, 7, 11]. Because of these two reasons it is felt that hydrogen embrittlement cannot be fully understood by the reduction of the surface energy due to adsorbed hydrogen.

A realistic treatment of the interaction between dislocation emission and bond breaking for a stable growing crack to obtain the measured dependence of a_n^H on pressure and temperature is well beyond current theoretical capabilities. The quantitative description of our measurements of a_n^H as a function of temperature and pressure gives some hints, how to tackle the problem. The function of equations (2) and (4)

$$X/(1-X) = k_0' \sqrt{p\,H_2} \cdot \exp(U/kT) \qquad (6)$$

which describes our data quite accurately [$X = a_n^H/\beta$, (2)], governs the dissociative filling of sites with hydrogen atoms, i.e. it applies to the filling of deep traps, $X = n$, [42, 43], as well as to the fractional surface coverage, $X = \theta$, by adsorbed atoms [Langmuir isotherm, (4)]. Because the relevant quantities enter only in the combination $X/(1-X)$, saturation behaviour is guaranteed. In order to see whether our results correlate with one of these quantities, all relevant data were plotted together in Fig. 16. All of our data with $4 \leqslant a_n^H \leqslant 11$ are included and should lie on a straight line, if (2) would be exact. The straight line through the data is obtained from equa-

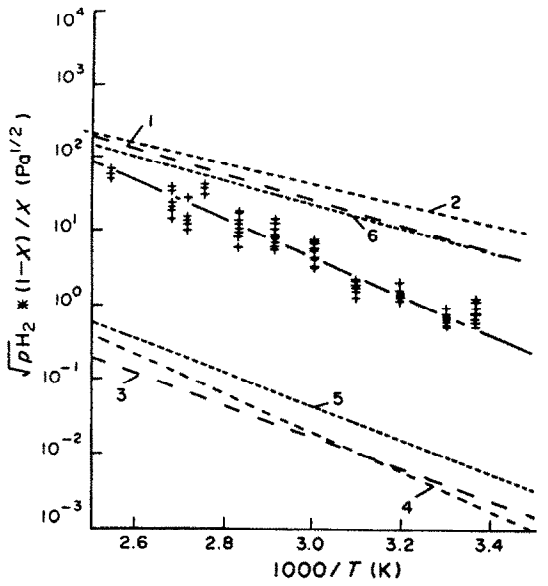

Fig. 16. Comparison of various quantities which all depend on pH_2 and T in the same way [equation (6)]. Data points and solid line: X = hydrogen embrittlement as measured by a_n^H/β. Curve 1,2: X = fractional coverage of deep traps (Refs [42,43]). Curve 3,4,5: X = hydrogen surface coverage (Refs 18,45,19]). Curve 6: X = hydrogen surface coverage if a O_2-adlayer is present (Ref. [19]).

tion (2) with the values of k_0 and U given in Table 1. This plot demonstrates that a single apparent activation energy describes the pH_2 and T dependence of a_n^H between $a_n^H = 4$ and $a_n^H = 11$ (see also Fig. 13). For comparison with these data the dependence of the fractional coverage of deep traps on pH_2 and T ($X = n$ in Fig. 16, curves 1 and 2) and the dependence of the hydrogen surface coverage θ ($X = \theta$ in Fig. 16, curves 3, 4, and 5) are drawn in the same diagram. The values of binding energies and pre-exponential factors used are given in Table 1. In addition, the diagram shows that the presence of an oxygen adlayer on the surface drastically decreases the coverage of adsorbed hydrogen (curve 6 vs curve 5 in Fig. 16).

The measured apparent activation energy for hydrogen assisted crack growth (slope of the data curve) agrees well with the isosteric heat of adsorption of hydrogen on Fe-(100)-surfaces (slope of curves 3 to 5) (see also Table 1). Therefore it is tempting to correlate hydrogen embrittlement with the surface coverage directly [27]. This is especially convincing, because the importance of the surface could be demonstrated by the oxygen experiments (see above). On the other hand the deviation of the absolute values due to large differences in the pre-exponential factor k_0 in equation (2) (see Table 1) are quite large. Therefore, it seems to be more appropriate to assume that our measurements indicate the filling of a trapping site, which is neither a surface site nor a deep trap in the bulk. It is most natural to assume, that this site is located right at the crack tip, where hydrostatic tension is so large, that continuum models predict $c_H = 1$ or where in other models the bonds are "most highly strained". In other words, we propose that the measured embrittlement is linearly related to the fractional coverage of sites in the core region of the crack $a_n^H = 2c/\delta \cong \beta \cdot n$ where n is the fractional coverage of these sites. The large concentration of hydrogen at the very crack tip reduces the cohesion forces as was postulated by Oriani [44]. The coverage of these sites must depend on the stress at the crack tip. In the examined temperature range the net stress decreases only by 5% with increasing pressure and temperature. Therefore it is assumed that due to dislocation screening a nearly constant stress state is maintained at the crack tip. Only for the highest temperatures examined a_n decreases with decreasing rate (Fig. 9b, 373 K). For these high temperatures the nucleation of dislocations is favored [14] as well as the stress might become too low to maintain a constant coverage at the tip.

It is felt, that all observations fit at least qualitatively into such a picture: oxygen does not embrittle since, although it adsorbs at the flat surface, its atoms are too large to be trapped at the postulated crack tip site. The most important reservoir, from which the growing crack tip receives the hydrogen, is the surface covered with adsorbed hydrogen. If this reservoir is blocked by oxygen, embrittlement is drastically reduced immediately. Temperature and pressure dependence are given by equation (2) with the measured values for k_0, U, β.

Rather involved theories are necessary for a whole lot of unsolved problems: characterization of the trapping site at the loaded crack tip, which emits or receives dislocations at a rather well defined rate (reproducible finite value of a_n^H) as well as cluster calculations to analyse the catalytic role of hydrogen in reducing the cohesive strength.

SUMMARY

An experimental method is described for measuring the crack tip opening angle, α, of a stable growing crack as a function of hydrogen pressure, pH_2, temperature, T, and crack tip opening rate, $\dot{\delta}$. This angle is used to characterize hydrogen assisted crack growth.

In single crystals three regions can be distinguished, a low temperature region where α decreases with decreasing rate, a high temperature region where the invers rate behaviour is observed and a region of intermediate temperatures where α is independent of $\dot{\delta}$.

In the intermediate region ($300\,K \leqslant T \leqslant 390\,K$) a single relationship describes the dependence of α on T and on pH_2 between $pH_2 = 10\,mPa$ and $pH_2 = 100\,kPa$.

Fractographic examinations as well as examinations of the influence of hydrogen–oxygen mixtures on the fracture process show that the hydrogen atoms act directly at the tip and are mainly supplied by surface diffusion from adjacent parts of the frac-

ture surface. The crack grows in a stable manner down to a scale of at least 100 nm by micro-cleavage and concomitant dislocation emission from the tip.

A quantitative comparison between the surface coverage of hydrogen on single crystal surfaces, the fractional coverage of volume traps and the observed dependence of α on $p\,H_2$ and T yields that hydrogen assisted crack growth in FeSi single crystals depends on the fractional coverage of special crack tip sites with a fractional coverage between that of surface sites and that of deep trapping sites but with the same apparent binding energy as the isosteric heat of adsorption of hydrogen on Fe-(100) surfaces.

Acknowledgement—Financial support by the Deutsche Forschungsgemeinschaft under contract number Ne 193/7 and Ne 193/9 is gratefully acknowledged.

REFERENCES

1. H. G. Nelson and D. P. Williams, NACE5, Unieux Firminy, France, p. 390 (1977).
2. R. P. Gangloff and R. P. Wei, *Metall. Trans. A* **8A**, 1043 (1977).
3. C. J. McMahon, *Hydrogen in Metals* edited by I. M. Bernstein and A. W. Thomson), p. 219. Am. Inst. Min. Engrs, New York (1981).
4. R. H. Jones, S. M. Brummer, M. T. Thomas and D. R. Baer, *Hydrogen in Metals* (edited by I. M. Bernstein and A. W. Thomson), p. 369. Am. Inst. Min. Engrs, New York (1981).
5. R. Thomson, *J. Mater. Sci.* **13**, 128 (1978).
6. J. E. Sinclair and M. W. Finnis, *Harwell Progress Report* AERE-PRI/TP 38, 10/80-9/81, 78 (1982).
7. J. R. Rice, *J. Mech. Phys. Solids* **26**, 61 (1978).
8. W. W. Gerberich and A. G. Wright, *Proc. Int. Conf. of Env. Degradation of Engng Mat. in Hydrogen*, p. 183. Blacksburg (1981).
9. R. A. Oriani and P. H. Josephic, *Acta metall.* **25**, 979 (1977).
10. J. P. Hirth and J. R. Rice, *Metall. Trans. A* **11A**, 1501 (1980).
11. B. S. Majumdar and S. J. Burns, *Acta metall.* **29**, 579 (1981).
12. J. Weertman, *Acta metall.* **26**, 1731 (1978).
13. R. M. Thomson and J. E. Sinclair, *Acta metall.* **30**, 1325 (1982).
14. H. Vehoff and P. Neumann, *Acta metall.* **28**, 265 (1980).
15. D. P. Williams and H. G. Nelson, *Metall. Trans.* **1**, 63 (1970).
16. R. W. Pasco and P. J. Ficalora, *Scripta metall.* **15**, 1019 (1981).
17. R. P. Wei, *Hydrogen in Metals* edited by I. M. Bernstein and A. W. Thomson), p. 677. Am. Inst. Min. Engrs, New York (1981).
18. F. Boszo, G. Ertl, M. Grunze and M. Weiss, *Appl. Surf. Sci.* **1**, 103 (1977).
19. J. Benzinger and R. J. Madix, *Surf. Sci.* **94**, 119 (1980).
20. K. Christmann, *Z. Naturforsch.* **34a**, 22 (1979).
21. R. M. McMeeking and D. M. Parks, ASTM STP 668, 175 (1979).
22. P. Neumann, *Acta metall.* **22**, 1167 (1974).
23. H. Vehoff and P. Neumann, *Acta metall.* **22**, 915 (1979).
24. S. P. Lynch, *Scripta metall.* **13**, 1051 (1979).
25. M. H. Kamdar, *Second Int. Cong. of Hydrogen in Metals*, H2, 3D10 (1977).
26. P. Neumann, H. Fuhlrott and H. Vehoff, ASTM STP 675, 371 (1978).
27. H. Vehoff, W. Rothe and P. Neumann, *ICF5 Cannes*, **1**, 265 (1981).
28. F. A. McClintock, *Int. J. Fract. Mech.* **4**, 101 (1968).
29. S. P. Lynch, *ICF5 Cannes* **1**, 254 (1981).
30. S. P. Lynch, Aeronautical Research Lab., Melbourne, private communication.
31. J. R. Griffith and D. R. J. Owen, *J. Mech. Phys. Solids* **19**, 419 (1971).
32. E. M. Riecke, MPI f. Eisenforschung, Düsseldorf, private communication.
33. W. M. Robertson, *Z. Metallk.* **64**, 436 (1973).
34. H. H. Johnson, *Hydrogen in Metals* (edited by I. M. Bernstein and A. W. Thompson), p. 35. Am. Soc. Metals (1974).
35. M. Kurkela and R. M. Latanision, *Scripta metall.* **13**, 927 (1979).
36. J. K. Tien, S. V. Nair and R. R. Jensen, Ref. **3**, 37 (1981).
37. E. Fromm and E. Gerbhardt, *Gase und Kohlenstoff in Metallen*, p. 583. Springer, Berlin (1976).
38. J. P. Hirth and B. Carnahan, *Acta metall.* **26**, 1795 (1978).
39. R. Gomer, R. Wortman and R. Lundy, *J. chem. Phys.* **26**, 1147 (1957).
40. J. R. Rice and R. Thomson, *Phil. Mag.* **29**, 73 (1974).
41. N. Petch, Phil. Mag. **1**, 331 (1956).
42. A. J. Kumnick and H. H. Johnson, *Acta metall.* **28**, 33 (1980).
43. E. M. Riecke, *Third Int. Cong. on Hydrogen and Materials*, H3, Paris, E7 (1982).
44. R. A. Oriani, *Ber. Bunsenges.* **76**, 848 (1972).
45. M. R. Shanaberger, *Hydrogen in Metals* (edited by J. M. Bernstein and A. W. Thomson), p. 135. Am. Inst. Min. Engrs, New York (1981).